Modeling Near-Edge Fine Structure X-ray Spectra of the Manganese Catalytic Site for Water Oxidation in Photosystem II

Barbara Brena,*,[†] Per E. M. Siegbahn,[‡] and Hans Ågren[§]

[†]Department of Physics and Astronomy, Uppsala University, Box 516, SE-75120 Uppsala, Sweden

[‡]Department of Physics, Alba Nova, and Department of Biochemistry and Biophysics, Arrhenius Laboratory, Stockholm University, SE-106 91, Stockholm, Sweden

[§]School of Biotechnology, Theoretical Chemistry and Biology, Royal Institute of Technology, S-106 91 Stockholm, Sweden

Ⓢ Supporting Information
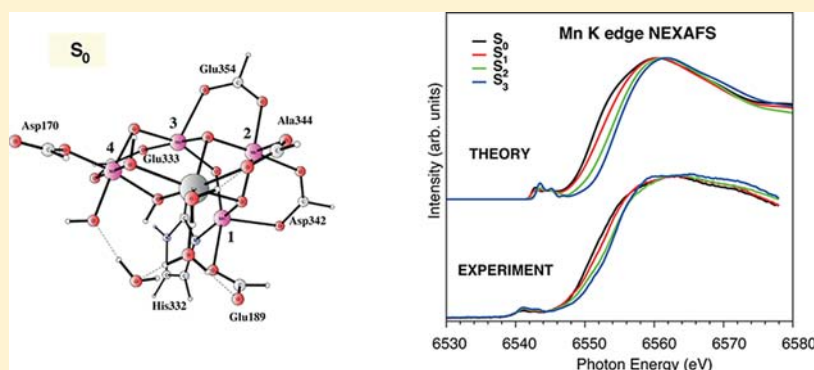
ABSTRACT: The Mn 1s near-edge absorption fine structure (NEXAFS) has been computed by means of transition-state gradient-corrected density functional theory (DFT) on four Mn_4Ca clusters modeling the successive S_0 to S_3 steps of the oxygen-evolving complex (OEC) in photosystem II (PSII). The model clusters were obtained from a previous theoretical study where they were determined by energy minimization. They are composed of Mn(III) and Mn(IV) atoms, progressing from $Mn(III)_3Mn(IV)$ for S_0 to $Mn(III)_2Mn(IV)_2$ for S_1 to $Mn(III)Mn(IV)_3$ for S_2 to $Mn(IV)_4$ for S_3, implying an Mn-centered oxidation during each step of the photosynthetic oxygen evolution. The DFT simulations of the Mn 1s absorption edge reproduce the experimentally measured curves quite well. By the half-height method, the theoretical IPEs are shifted by 0.93 eV for the $S_0 \rightarrow S_1$ transition, by 1.43 eV for the $S_1 \rightarrow S_2$ transition, and by 0.63 eV for the $S_2 \rightarrow S_3$ transition. The inflection point energy (IPE) shifts depend strongly on the method used to determine them, and the most interesting result is that the present clusters reproduce the shift in the $S_2 \rightarrow S_3$ transition obtained by both the half-height and second-derivative methods, thus giving strong support to the previously suggested structures and assignments.

INTRODUCTION

The use of X-ray spectroscopy is commonly motivated by the localized nature of the core electrons, which implies effective selection rules, valuable for mapping the electron distribution, and a chemical shift that carries conformational information. X-ray techniques have generally experienced a great revival in recent years owing to the technical development of light sources. It is now possible to correlate specific X-ray features with functional groups and even individual bonds, such that the total spectrum can be considered as a linear combination of elementary spectra: the "building block principle".[1−5] In addition to applications of this principle and other rules of thumb, the general development in simulation technology has made it possible to address ever-larger systems with complex X-ray spectra, such as biological molecules. Thus, computational studies of the near-edge X-ray absorption fine structure (NEXAFS) spectra of amino acids and polypeptides in solution or on surfaces have become common practice.[6−9] Moreover,

structures like proteins, polynucleotides, and DNA are nowadays addressed,[10−15] demonstrating the ability of computations to identify particular amino acids and to use their characteristic features for chemical mapping. Computational analysis has helped to identify the origin of individual peaks, and the spectroscopic assignments are obtained in terms of hydrogen bonds, tautomerism, and stacking, to such an extent that absorption spectroscopy even can be utilized to refine particular structures of DNA as obtained from X-ray crystallography.[16]

Our present work takes account of the aforementioned development of X-ray simulations of complex biosystems and addresses the K-edge NEXAFS spectra of the manganese complex of photosystem II (PSII), where water oxidation takes place. PSII is a multiprotein enzyme situated in the thylakoid

membrane of plants, algae, and cyanobacteria. The oxygen-evolving complex (OEC) contains four manganese atoms and one calcium atom connected by μ-oxo bridges. X-ray diffraction studies during the past seven years have considerably clarified the detailed structure of the OEC.[17−19] In the first of these studies,[17] it was shown that three of the manganese atoms and the calcium atom form a cuboidal structure, with the fourth manganese atom situated outside the cube. The amino acids most likely to be ligated to the complex were also assigned. Waters were assumed to fill up the remaining coordination sites. Since the resolution was rather low (3.5 Å), the positions of the bridging oxo groups and the metal connectivity of the ligands could only be assumed. In more recent X-ray structures, the resolution was slightly higher (2.9−3.0 Å),[18,19] and a different ligation pattern was suggested, partly based on chemical intuition, with most of the carboxylate amino acid ligands assumed to bind bidentately between two different metal atoms. This meant that hardly any water-derived ligands had to be added to saturate the metal coordination. The positions of the metal atoms were similar to the ones in the earlier X-ray structure, with the exception of the outside manganese, which was placed farther out from the Mn_3Ca cube. No positions for the oxo groups were suggested. Quite recently, a new high-resolution (1.9 Å) X-ray structure was obtained, which turned out to be very similar to a previously suggested structure obtained from calculations using density functional theory (DFT).[20] A simplified model of that theoretical structure has been used here for the NEXAFS analysis.

In the present study, we make use of NEXAFS as an element-specific spectroscopic technique, to investigate the electronic structure of the excited atoms and the character of the OEC states, and, in particular, of special interest for this case, we analyze and exploit the spectral sensitivity to oxidation states of the different manganese atoms involved in the complex. Water oxidation involves four flash-induced steps with intermediates denoted as S_0 to S_4, according to a scheme proposed by Kok et al.[21] In each of the steps an electron is released from the OEC, in most cases together with a proton, and O_2 is formed in the last step.

A good starting point for discussion of the present results is the review by Yano and Yachandra,[22] in which the resolution capability of X-ray absorption spectra of manganese clusters at the K-edge was demonstrated and used to build a structural model for evolution of the cluster during the photosynthesis process. Yachandra et al.[23] summarized data of K-edge absorption of the OEC and could, together with electron paramagnetic resonance (EPR) data, draw a number of conclusions on the cluster structure, in particular on the oxidation states of the metals. Concomitant computational work has since then been carried out. Examples are the recent studies by Jaszewski et al.,[24,25] in which the manganese complexes were studied with different ligand environments by use of time-dependent density functional theory (TDDFT) and where different oxidation states were correlated with the positions of the Mn K-edges.

A key issue of particular importance in the present context is whether a manganese- or a ligand-centered oxidation occurs in the $S_2 \rightarrow S_3$ transition. In one set of studies,[23,26] it was concluded that the most likely assignment of this oxidation was a bridging μ-oxo group. This conclusion was based on a combination of results from NEXAFS, extended X-ray absorption fine structure (EXAFS), and $K\beta$ X-ray emission spectroscopy (XES) measurements. In another set of quite similar studies, it was instead concluded that the oxidation should be manganese-centered.[27] The most recent DFT studies have supported the latter assignment.[28]

In the following we outline the main characteristics of the theoretical model employed for X-ray absorption spectra, in particular considering complex systems of the type studied here. In order to explore the possibilities of our X-ray simulation technology and to validate parametrizations—density functionals, basis set, and structural models—we carried out a set of calculations on some manganese-containing complexes and compared the results with available high-resolution experimental spectra. In the next section we subsequently discuss the calculated results in relation to the oxidation state assignment. We thereafter discuss our results both in view of earlier spectroscopic work and in a general context of assessing the structure and functionality of the OEC, in the Discussion section. Some general conclusions end the paper.

COMPUTATIONAL METHODS

NEXAFS spectroscopy reflects the promotion of a core electron into an unoccupied level in the discrete or continuum parts of the N-electron spectrum. A variety of methodologies have been developed to compute such spectra, a few with the capability to address systems of the complexity and size that are studied in the present work. We use transition-state theory, originally introduced by Slater,[29] and employed for X-ray and photoelectron spectroscopies over a long time, and which has been implemented in modern density functional theory by Chong,[30] Stener et al.,[31] and Triguero et al.[32] With transition-state theory, one obtains the relaxation contribution to the binding energy up to second-order in the energy for self-consistent field optimization between ground and core hole states (ΔSCF method). Maintaining orbital orthogonality and with the spectral energies obtained as differences of transition-state orbital energies, the transition-state method allows a very effective construction of X-ray spectra while still maintaining an accuracy that matches ΔSCF (ΔKohn−Sham) and "static exchange" levels of theory very well. For benchmarks, one can refer to studies on small molecules,[32] fullerenes,[33] and solutions.[34,35]

In the discrete part of the spectrum, the transition state eigen-pairs of excitation energies and moments provide a true spectral representation, while in the continuum they do not represent a correct normalization. However, closely above the ionization potential, the deviation from the true normalized spectrum is still minor,[36] growing progressively poorer for higher energies covering shape resonance and multiple scattering regions. By experience, close to the ionization potential the continuum smearing effect can be caught by empirical broadening of the primitive spectrum; see further below.

In the present paper we study the NEXAFS K-edge spectrum of manganese, reflecting the promotion of the manganese 1s orbital electron into unoccupied levels of the full cluster. The transition is in the range of 6 keV with a broadening of the 1s level of 1.0 eV. There is thus a considerable smearing-out of structures also of the discrete part of the NEXAFS spectrum compared to low-Z compounds. Another difference with respect to the latter is a strong relative enhancement of the near ionization potential region (and beyond) in relation to the discrete part of the spectrum. Combined with the large lifetime broadening, this makes the edge region close to the ionization potential, and in particular the inflection point of the spectrum at the edge, the most suitable region in the search for structure−property relationships. We will therefore here explore the relationship between inflection point energy (IPE) and oxidation state.

NEXAFS Mn K-edge spectra were generated for Mn in different oxidation states by considering Mn(II), Mn(III), and Mn(IV) reference compounds, for which high-quality experimental spectra are available. These complexes, each containing a single Mn atom, are $Mn(II)(acac)_2(H_2O)_2$, $Mn(III)(acac)_3$, and $Mn(IV)(sal)_2(bipy)$, where acac = acetylacetonate, sal = salicylate, and bipy = bipyridine.

17158

dx.doi.org/10.1021/ja306794p | *J. Am. Chem. Soc.* 2012, 134, 17157−17167

The same molecules have been used as test models for experimental measurements by Yachandra et al.[37] The structures of the molecules were optimized by using the Gaussian 09 program[38] at the B3LYP[39] level with the 6-31G(d,p) basis set.

The geometry-optimized structures are shown in Figure 1. The charges on each complex are +2 for Mn(II), +3 for Mn(III), and 0 for
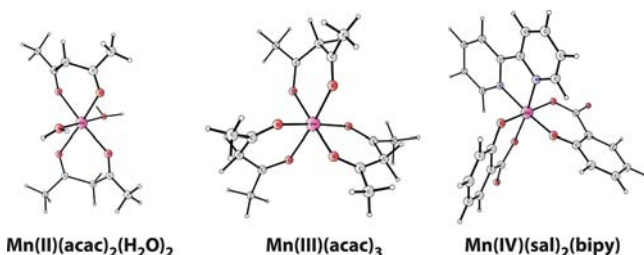
Figure 1. Structures of reference compounds Mn(II)(acac)$_2$(H$_2$O)$_2$, Mn(III)(acac)$_3$, and Mn(IV)(sal)$_2$(bipy).

Mn(IV). The total spin (S) of each molecule is $^5/_2$ for Mn(II), 2 for Mn(III), and $^3/_2$ for Mn(IV). In all complexes the Mn is hexacoordinated. In Mn(aII)(acac)$_2$(H$_2$O)$_2$, the distance between Mn and the four O of the acetylacetonate ligands amounts to 2.15 and 2.16 Å, while the distance to the water ligands is 2.26 Å. In Mn(III)(acac)$_3$ the distances to the six acetylacetonate ligands are 1.96, 1.96, 1.99, 2.02, 2.15, and 2.15 Å . In Mn(IV)(sal)$_2$(bipy), the distance of Mn from pyridine C is 2.01 Å, and the distances of Mn from the four salicylate O are 1.92, 1.92, 1.95, and 1.95 Å.

Since the recent high-resolution structure of PSII[40] was not available at the start of the present project, the model structures of the different S states were taken from earlier model calculations.[28] The models were furthermore reduced to fit present capabilities for NEXAFS calculations. This meant that only ligands directly bound to the OEC were kept, which is in line with the notion of the local electronic structure dependence of X-ray transitions. The carboxylate-containing ligands (aspartate and glutamate) were modeled by formate, and histidine was modeled by imidazole. The glutamine was replaced by water. After the truncation, the structures were fully optimized at the B3LYP level by use of the LACVP*[41] basis set. Structures are given in the Supporting Information. The total spin and charge of S$_0$, S$_1$, S$_2$, and S$_3$ compounds are summarized in Table 1.

Table 1. Total Spin and Charge of Tetranuclear Mn Clusters S$_0$ through S$_3$

	spin	charge
S$_0$	7.5	−2
S$_1$	7.0	−2
S$_2$	6.5	−1
S$_3$	6.0	−1

The NEXAFS Mn K-edge spectra of Mn complexes and of Mn tetranuclear intermediates S$_0$ through S$_3$ were calculated with the DFT code StoBe.[42] We have used the generalized gradient-corrected exchange functional by Becke[43] and the correlation functional by Perdew.[44] StoBe uses a double basis set technique to minimize the energy and an augmented diffuse basis set (19s, 19p, 19d) to calculate excitation energies and transition moments in the core-excited atoms.[45] The ionization potentials for Mn 1s electrons were calculated according to the ΔKohn−Sham approach as the difference in total energy between compounds in the ground state and in the presence of a Mn 1s core hole. The different electronic configurations were energy-optimized. The IGLOO-III triple-ζ basis of Kutzelnigg et al.[46] was employed for describing the core excited Mn atoms. For the other atoms, we used triple-ζ plus valence polarization basis sets provided by the StoBe package. In the calculations of the S$_0$ through S$_3$ clusters, the remaining three Mn atoms not core excited were represented by an

effective core potential of 13 electrons provided by the StoBe package. The total Mn K-edge spectrum of each tetranuclear Mn complex is the result of the summation of spectra computed for each Mn atom of the complex.

The simulated absorption spectra obtained for the Mn(II), Mn(III), and Mn(IV) reference compounds were convoluted with Gaussian curves of full width at half-maximum (fwhm) of 1.5 eV up to the energy position of the top of the adsorption edge. The fwhm was then linearly increased up to 20 eV over an energy interval of about 45 eV. Each simulated spectrum of the S$_0$, S$_1$, S$_2$, and S$_3$ clusters was convoluted by a Gaussian curve of 1.0 eV fwhm up to the ionization potential and linearly increased up to 20 eV in an interval of about 55 eV. Each single Mn spectrum was aligned to the IP calculated with the Δ KS approach. The total computed spectra of S$_0$ through S$_3$ were normalized to their own maximum intensities. Thereafter, all the computed NEXAFS energies are shifted by the same amount of 34.6 eV, so that the energy scale of the theoretical curves is aligned with the experimental spectra, and this includes also the relativistic shift. We have set the energy of the half intensity of the edges of the S$_0$ theoretical and experimental curves to coincide. By shifting all the theoretical curves by the same amount, the relative shifts between the absorption edges obtained in the calculations are preserved. Neglect of relativistic effects implies a shift of the spectral onset, which is a few tenths of an electronvolt for common organic NEXAFS spectra but which for manganese 1s IP is on the order of about 40 eV. Thus, this contribution is very chemically inert for manganese atoms of different electronic structure environments. The contribution to the IP shifts due to different chemical structure can mainly be divided into an initial potential (electrostatic) effect and a final polarization effect.[47,48] For charged or polar neutral compounds, the largest contribution originates from the former effect, which also varies most with conformation or substitution, while the final state polarization, the major contribution for nonpolar systems, is relatively constant and can often be estimated by pure dielectric models. By experience, our contention is that the present clusters are sufficiently large to well accommodate both these major contributions, maybe except the small fraction of long-distance final state polarization, which, however, is common to all states/models.[49] Further common shifting includes systematic errors and basis-set and functional incompleteness common to all atoms/states, thereby laying free the IP dependence on ligand electronic structure and oxidation state.

■ RESULTS

NEXAFS K-Edge Spectra of Reference Mn Compounds. In order to validate our methodology, we first address NEXAFS K-edge spectra of the three reference Mn compounds. In general, the oxidation states of the Mn atoms depend on the types of ligands and on the total spin and charge of the complex. To determine the oxidation states of each of the Mn atoms in the compounds studied, we have analyzed the Mulliken spin populations computed by the StoBe code for each Mn.[50,51] Specifically, the Mn atom in the Mn(II)-(acac)$_2$(H$_2$O)$_2$ complex has a spin population of 4.86 electrons, and according to ref 51 this value can be ascribed to an oxidation state of II. The Mn in Mn(III)(acac)$_3$ has a spin population of 4.06 electrons and is assigned to an oxidation state of III, and the Mn in Mn(IV)(sal)$_2$(bipy) has a spin population of 2.85 electrons and oxidation state IV.

In Figure 2 the computed Mn K-edge NEXAFS spectra of the Mn(II), Mn(III), and Mn(IV) reference compounds are shown. The Mn K-edge NEXAFS implies mainly transitions of 1s electrons into the 4p levels, but also the 3d levels are involved. The spectra are characterized by a main threshold around 6545−6555 eV, given by excitations of the Mn 1s electrons into the 4p unoccupied levels. In the spectra presented in Figure 2 the IPE can be coupled to the oxidation state of the Mn atoms, as has been previously shown by several
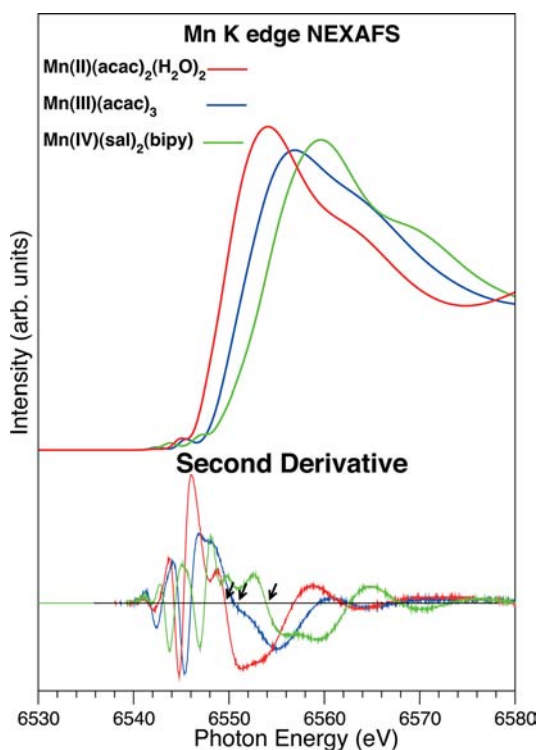
Figure 2. Theoretical Mn K-edge NEXAFS of the mononuclear reference compounds $Mn(II)(acac)_2(H_2O)_2$, $Mn(III)(acac)_3$, and $Mn(IV)(sal)_2(bipy)$. The computed second derivative for each spectrum is shown in the lower part of the figure. Arrows indicate the zero intersection of the second derivative.

measurements on different complexes containing Mn in different oxidation states.[52] In our computed spectra, the absorption threshold shifts toward higher energies as the oxidation state of the Mn atom increases, in good agreement with the experimental results for the same compounds performed by Yachandra et al.[53] The energy position of the threshold, which varies considerably in the three cases, is in fact translated toward increasing energies starting from $Mn(II)$-$(acac)_2(H_2O)_2$ to $Mn(III)(acac)_3$ and to $Mn(IV)(sal)_2(bipy)$, as is evident from a visual comparison. The IPE was estimated by two methods. The first method is as the energy at half intensity of the rising curve, with the following results: 6549.4 eV for $Mn(II)(acac)_2(H_2O)_2$, 6551.2 eV for $Mn(III)(acac)_3$, and 6553.5 eV for $Mn(IV)(sal)_2(bipy)$. The IPE difference between $Mn(II)(acac)_2(H_2O)_2$ and $Mn(III)(acac)_3$ amounts to 1.8 eV, and between $Mn(III)(acac)_3$ and $Mn(IV)(sal)_2(bipy)$ the difference is 2.3 eV. With the IPE estimated as the zero crossing of the second derivative of the absorption threshold, we have obtained 6549.6, 6550.5, and 6553.9 eV respectively, with differences of 0.9 and 3.4 eV. The accuracy in determining the shifts from the theoretical curves with the chosen broadening procedure is about ±0.1 eV. The shifts are thus completely different depending on the method used to define them, the half-height or the second-derivative method. This has to be borne in mind when the results below are analyzed.

At lower energies, starting above 6540 eV and extending toward the threshold, a number of low-intensity peaks form the so-called pre-edge region. These features originate from 1s excitations into the not fully occupied 3d levels of Mn. While the absorption edge is mainly assigned to dipole-type excitations, the pre-edge peaks are usually interpreted by

quadrupole transitions of 1s into 3d levels. However, in the presence of symmetry breaking, the mixing of 3d and 4p orbitals can occur and transitions into these 3d–4p states can be allowed even in a dipole calculation, like in our case.[54] The pre-edge peaks in our calculations are located at energies that are closer to the edge with respect to the experimental spectra.

NEXAFS K-Edge Spectra of Models of the Mn$_4$ Complex. In Figure 3, an atomic model of the tetranuclear
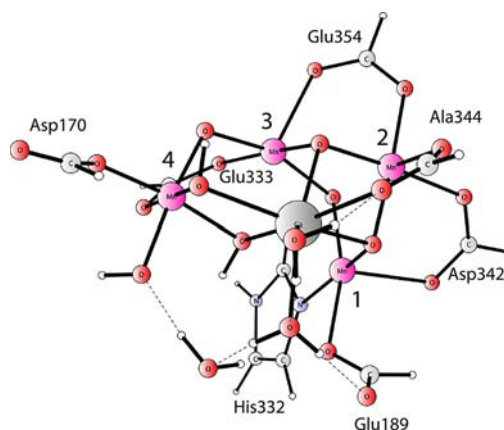
Figure 3. Structure of tetranuclear Mn model complex S_0.

Mn cluster used to simulate the S_0 model is shown, in which the positions where aspartate and glutamate were modeled by formate, histidine by imidazole, and glutamine was replaced by a water are indicated. In Table 2, the oxidation states of every

Table 2. Mullikan Spin Populations^a and Oxidation States of the Four Mn Atoms in Tetranuclear Mn Complexes Modeling States S_0 through S_3

	Mn1	Mn2	Mn3	Mn4
S_0	3.80, III	3.99, III	3.92, III	2.93, IV
S_1	3.80, III	3.95, III	2.95, IV	3.04, IV
S_2	3.90, III	3.06, IV	2.86, IV	3.01, IV
S_3	3.29, IV	3.15, IV	2.94, IV	3.02, IV

^{a}Expressed as the number of unpaired electrons.

Mn atom in each S complex are listed. As for the mononuclear complexes previously described, the oxidation states are deduced from the Mulliken spin population computed by the StoBe code on each Mn atom.[50]

In Figure 4A, the total Mn K-edge spectra computed for each complex are displayed together with the experimental data by Messinger et al.[26] As mentioned above, the theoretical curves are the sum of the NEXAFS results calculated for each of the four Mn in the complexes. The computed absorption edges of the model complexes S_0 through S_3 follow the same order as the experimental curves of the relative samples, with the edge of S_0 being the one at the lowest energy and the edge of S_3 at the highest energy. The general shape of the experimental profiles is overall well reproduced by the simulations, see Figure 4B, where the curvatures of the S_0 and S_1 spectra in the edge region match very well with the experiment. The computed spectra are also able to simulate the change in shape of the S_2 and especially of the S_3 state in the same interval in the measurements. The pre-edge region represented by the two peaks at about 6541 and 6543 eV in the experiments is reproduced in the simulation, although by a slightly more

17160

dx.doi.org/10.1021/ja306794p | J. Am. Chem. Soc. 2012, 134, 17157–17167
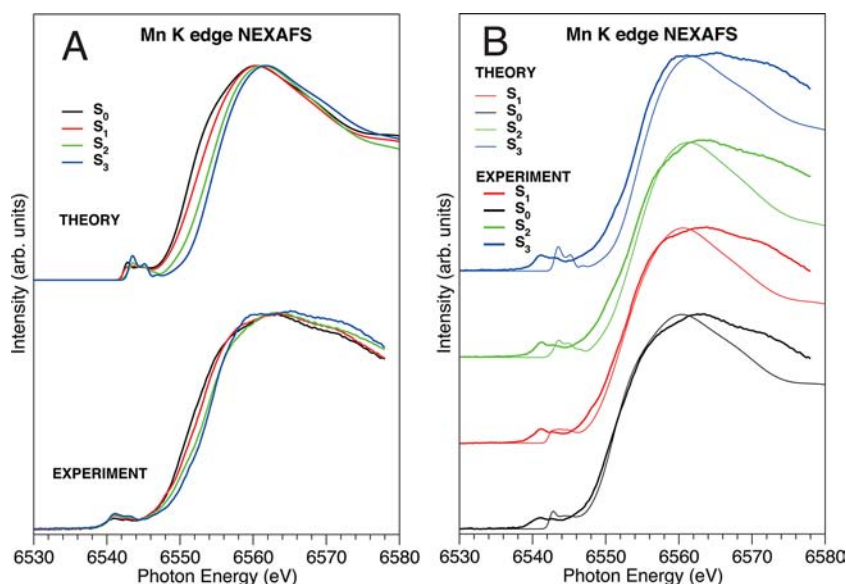
Figure 4. (A) Theoretical spectra of Mn K -edge NEXAFS of model complexes for the S_0, S_1, S_2, and S_3 states of PSII, in comparison with the experimental measurements of Messinger et al.[26] (B) Computed spectra superimposed on experimental ones.

complex group of peaks and at higher energies. In analogy with the experiment, the model complex for S_3 has the highest intensity pre-edge resonances at 6542.7 and 6544.5 eV, followed by S_2, with two resonances at 6543.6 and 6545.3 eV. S_1 and S_0 both have two peaks at 6542.7 and 6544.6 eV.

In Figure 5 the second-derivative and theoretical total spectra for S_0, S_1, S_2, and S_3 are displayed. The IPE values obtained as the zero crossing of the second derivative and those estimated by the half-height of the threshold of the normalized total spectra are listed in Table 3. As for the mononuclear Mn
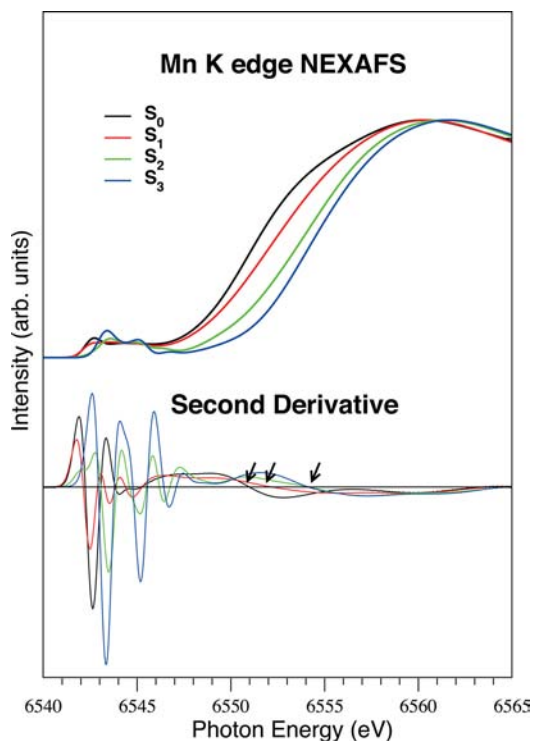
compounds described previously, the accuracy of the IPEs for the theoretical curves is about ±0.1 eV.

The single NEXAFS curves calculated for each of the four Mn atoms in the S_i clusters are displayed in Figure 6. A visual inspection shows that the edges of the spectra related to Mn atoms with oxidation states III and IV are energetically shifted from each other, constituting two distinct groups. However, individual differences can be seen in the energy position and in the fine structure of each curve. In Table 4 the edge energies estimated for each of the atomic Mn spectra of Figure 6 are listed. The IPEs were estimated both as the energy at half-height of the raising absorption edge of the single atom spectra, which were not normalized, and as the zero crossing of the second derivative. The IPEs obtained with the first method vary between 6550.13 and 6551.35 eV for Mn(III) and between 6554.00 and 6555.27 eV for Mn(IV). The variations are 1.22 and 1.27 eV, respectively. For the second method, the IPEs vary between 6549.97 and 6551.47 eV for Mn(III) and between 6553.42 and 6555.48 eV for Mn(IV). In this case the variations are between 1.50 and 2.06 eV, respectively.

■ DISCUSSION

Theoretical Results for Mn K-Edge NEXAFS. The sensitivity of the K absorption edge to the oxidation state is a known phenomenon observed in several elements, and it has been experimentally verified for Mn by a large number of studies. Our theoretical approach, based on transition-state gradient-corrected Kohn−Sham DFT, is clearly able to reproduce the measured increase of the absorption edge energy for samples containing Mn with higher oxidation states, as evidenced by Figures 2, 4, and 6. In general, previous experimental works have shown that a threshold shift to higher energy of about 1 up to 3 eV can be attributed to a higher oxidation state on one Mn atom of a unit.[52,55] Our computed absorption spectra of the mononuclear Mn(II), Mn(III), and Mn(IV) complexes, shown in Figure 2, clearly replicate this trend. The theoretical energy differences between Mn(II)-$(acac)_2(H_2O)_2$ and Mn(III)$(acac)_3$ and between the latter and Mn(IV)$(sal)_2(bipy)$ are 1.8 and 2.3 eV for the half-height

Figure 5. Second derivative of Mn K-edge NEXAFS of the model complexes S_0, S_1, S_2, and S_3. Arrows indicate the zero intersections.

Table 3. Inflection Point Energies for Model Complexes for States S_0 through S_3 and Their Differences in Transitions $S_0 \rightarrow S_1$, $S_1 \rightarrow S_2$, and $S_2 \rightarrow S_3$

	IPE, eV						
	S_0	S_1	S_2	S_3	$S_1 \rightarrow S_0$	$S_2 \rightarrow S_1$	$S_3 \rightarrow S_2$
half-height[a]	6551.55	6552.48	6553.91	6554.54	0.93	1.43	0.63
zero crossing[b]	6551.04	6552.21	6554.18	6554.18	1.17	1.97	0.00

[a]Estimated as the energy position at half intensity of the absorption threshold. [b]Estimated by zero crossing of the second derivative.
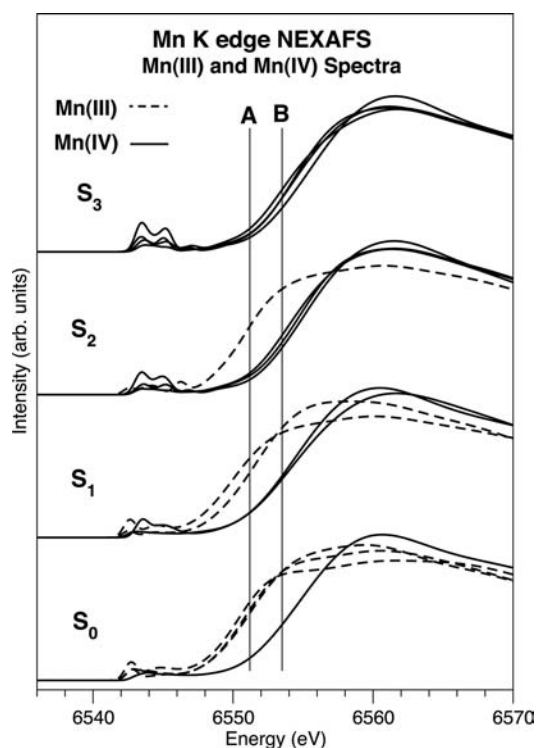
Figure 6. Theoretical spectra of Mn K-edge NEXAFS for each of the four Mn atoms of the model complexes S_0, S_1, S_2, and S_3. Spectra were computed for single Mn atoms with oxidation state (---) III and (—) IV. As a comparison, lines A and B are positioned at 6551.2 and 6553.5 eV, which are the theoretical IPEs of Mn(III)(acac)$_3$ and Mn(IV)-(sal)$_2$(bipy), respectively, computed as the energy of the half-height of the maximum intensity of the edge.

method. It has to be observed that when different complexes are compared, a precise quantitative correlation between the energy position of the absorption edge and the increase/decrease of the oxidation state is complicated by the presence of different ligands and is more difficult when multinuclear clusters are considered.[55]

To analyze how this topic affects our theoretical approach, we can consider the single atomic spectra of Figure 6. Overall, the NEXAFS spectra of each of the Mn(III) atoms are characterized by absorption edges lying at lower energies with respect to those of the Mn(IV) atoms. The estimated IPEs of the Mn(III) and Mn(IV) atoms are distributed over an energy interval of about 1.2 eV according to the half-height method (see Table 4). We have compared the IPEs computed for the mononuclear compounds to the atomic IPEs of Table 4. The IPE of the Mn(III)(acac)$_3$ compound lies at 6551.2 eV, and the IPEs of the various Mn(III) atoms in the S states are between 6550.1 and 6551.4 eV. The IPE of the Mn(IV)(sal)$_2$(bipy) compound lies at 6553.5 eV, and the IPEs of of the various Mn(IV) atoms in the S states are between 6554.0 and 6555.3 eV. This shows that in our DFT-computed spectra of the tetranuclear clusters the energy position of the edge is clearly sensitive to the Mn oxidation state, and the IPE positions are in agreement with those obtained for the mononuclear model compounds.

In Table 5 we have listed the experimental IPEs and the IPE differences obtained in previous experimental studies[26,27,56,57] in comparison with the theoretical values calculated in this work.

The experimental results summarized in Table 5 provide different pictures for the evolution of the S states. The half-height method gives reasonably stable shifts of about 1.0−1.3 eV for the $S_0 \rightarrow S_1$ and $S_2 \rightarrow S_3$ transitions and slightly smaller for the $S_1 \rightarrow S_2$ transition of 0.6−0.8 eV.[27,56] These results

Table 4. Inflection Point Energies of Each Single Mn Atom of the S_i Complexes[a]

	half-height				second-derivative			
	Mn1	Mn2	Mn3	Mn4	Mn1	Mn2	Mn3	Mn4
				S_0				
IPE, eV	6550.93	6551.22	6550.94	6554.45	6551.2	6550.32	6550.89	6554.84
oxidation state	III	III	III	IV	III	III	III	IV
				S_1				
IPE, eV	6550.13	6551.35	6554.28	6554.19	6549.97	6551.47	6554.06	6554.43
oxidation state	III	III	IV	IV	III	III	IV	IV
				S_2				
IPE, eV	6551.04	6554.53	6554.14	6555.00	6550.88	6554.70	6553.87	6554.94
oxidation state	III	IV	IV	IV	III	IV	IV	IV
				S_3				
IPE, eV	6554.41	6554.00	6554.28	6555.27	6554.14	6554.22	6553.42	6555.48
oxidation state	IV	IV	IV	IV	IV	IV	IV	IV

[a]The energies are estimated by the energy position at half intensity of the absorption threshold and as the zero crossing of the second derivatives. The oxidation states are also indicated.

Table 5. Inflection Point Energies Reported in Experimental Studies for S_i Samples and Obtained from DFT Calculations in This Work, and Their Differences in Transitions S_0 to S_1, S_1 to S_2 and S_2 to S_3[a]

	IPE, eV						
ref	S_0	S_1	S_2	S_3	$S_1 \to S_0$	$S_2 \to S_1$	$S_3 \to S_2$
			Experiment				
56[b]	6550.7	6551.7	6552.5	6553.7	1.0	0.8	1.2
57[c]	6550.1	6551.7	6553.5	6553.8	1.6	1.8	0.3
27[d]		6551.9			1.0	0.6	1.0
27[c]		6553.0			2.4	0.8	0.7
27[e]		6551.3			1.1	0.7	1.1
27[b]		6552.8			1.3	0.8	0.8
26[c]	6550.8 ± 0.1	6552.9 ± 0.1	6554.0 ± 0.1	6554.3 ± 0.1	2.1	1.1	0.3
			Theory				
this work[b]	6551.55	6552.48	6553.91	6554.54	0.93	1.43	0.63
this work[c]	6551.04	6552.21	6554.18	6554.18	1.17	1.97	0.00

[a]The IPE was estimated by different methods in different works, as indicated. [b]Half the peak height. [c]Zero intersection of the second derivative. [d]Integral method. [e]Half the normalized height.

suggest quite clearly that there are manganese oxidations in all three transitions. A disturbing point is that the shifts in the mononuclear reference compounds were about twice as large, showing influences of the other manganese and possibly different ligand effects in the Mn_4 complex. In contrast, the second-derivative method gives a more shattered picture with 1.6−2.4 eV for the $S_0 \to S_1$ transition, 0.8−1.8 eV for the $S_1 \to S_2$ transition, and only 0.3−0.7 eV for the $S_2 \to S_3$ transition.[26,27,57] These latter results were interpreted to suggest a ligand oxidation in the $S_2 \to S_3$ transition, in line with other results from EPR and X-ray absorption spectroscopy.[26,57] Due to these different interpretations and other results, the character of the $S_2 \to S_3$ transition has been one of the most debated steps in the photosynthetic reaction sequence, and it is still somewhat controversial. The oxidation-state sequence is thus S_0 (III, III, III, IV) $\to$ S_1 (III, III, IV, IV) $\to$ S_2 (III, IV, IV, IV) $\to$ S_3 (IV, IV, IV, IV) in the former proposal and S_0 (III, III, IV, IV) $\to$ S_1 (III, III, IV, IV) $\to$ S_2 (III, IV, IV, IV) $\to$ S_3 (III,IV,IV,IV) in the latter. The latter assignment was also supported by $K\beta$ XES measurements, and an analysis of the reasons that might have caused different IPE shifts is given in previous studies.[26] In general, the results of the experiments critically depend on the decomposition in S states of the flash samples. It was argued that different deconvolution procedures could be the origin of the differences to Roelofs et al.[57] and Iuzzolino et al.,[27] while Ono et al.[56] did not provide a characterization of the S-state composition.

The present computational analysis starts at the other end compared to the experiments. The clusters chosen for the different S states were here obtained from an energy-minimization procedure[28] and all of them have well-defined oxidation states showing Mn oxidation in each S-state transition. The IP shifts are computed by both the half-height and second-derivative methods, and the main question is whether the absence of shift by the second-derivative method necessarily indicates an oxidation of a ligand rather than manganese, as suggested by Roelofs et al.[57]

According to our theoretical absorption spectra for the model clusters, and considering the IPEs obtained at half the normalized height, the $S_0 \to S_1$ transition has a shift of 0.93 eV, with the $S_1 \to S_2$ transition of about 1.43 eV. Finally the shift in the $S_2 \to S_3$ transition is slightly smaller, amounting to 0.63 eV. The results must be concluded to agree reasonably well with the experimental results. However, some of the details are not

the same, showing the difficulty in obtaining theoretical spectra of very high accuracy. Very interestingly, the shift in the $S_2 \to S_3$ transition by the second-derivative method is absent (0.0 eV), in line with the small result of only 0.3 eV obtained experimentally by this method. The conclusion is clear: the absence of a shift by the second-derivative method does not necessarily exclude a manganese oxidation.

The analysis of spectral decomposition of Figure 6 clarifies the range of IPE differences obtained in our simulations. As previously noted, each theoretical single Mn absorption spectrum is characterized by a slightly different IPE and by a specific fine structure, determined by its local chemical environment, as shown in Figure 6. These features vary among the single Mn atoms and clusters. The total final profile for each S state is influenced by the fine structure of the contributing atomic spectra, and this complicates the assignment of the Mn oxidation states in the tetranuclear complexes.

From Figure 6, one can see how the total spectra are affected by the changes of the atomic profiles in the vicinity of the threshold region. One can observe in Figure 4A, where the absorption spectra of the clusters S_0, S_1, S_2 and S_3 are displayed on top of each other, that just before the edge the experimental thresholds of the spectra of S_2 and S_3 increase in intensity more slowly than the thresholds of S_1 and S_0, resulting in different curvatures. The same effect is obtained in the theoretical simulations and is determined by the amount of Mn(III) and Mn(IV) in each cluster. Due to the energy shifts of the edges, in the energy region at the lower part of the edge, around 6550 eV and below, the total NEXAFS curves have higher intensity the more Mn(III) are present in the cluster, and on the contrary, lower intensity the more Mn(IV) are present in the cluster.

Dau et al.[58,59] addressed the role of coordination and oxidation on the shapes of NEXAFS spectra by analyzing results from MSX_α simulations for single-metal manganese−water complexes. They concluded that the changes in the shape of the edge spectra observed for the $S_2 \to S_3$ transition are explainable by the transformation from five-coordinated Mn(III) to six-coordinated Mn(IV) complexes and that these changes therefore are associated with oxidation of a manganese atom rather than a ligand. This is an important observation made long before a high-resolution X-ray structure was available, and it is strongly supported by later DFT studies based on energy minimizations.[20,28] These authors speculated

that the higher coordination changes the local manganese p- versus d-orbital contributions to unoccupied molecular orbitals at the edge, thereby shifting the apparent absorption spectrum as governed by local X-ray selection rules (here s − p). They also discussed an indirect effect of coordination in the change of bond length and thereby IPE shifts due to changes in the "particle in the box" potential.

The simulated shift of $S_2 \rightarrow S_3$ in Dau's analysis[58,59] was about a factor of 4 larger than that observed experimentally, something that was explained by the fact that only one of the four manganese atoms is oxidized in this transition. This holds, of course, for any of the single oxidation steps, and the fact that the $S_2 \rightarrow S_3$ edge shift is significantly smaller in our calculations than the $S_0 \rightarrow S_1$ and $S_1 \rightarrow S_2$ shifts calls for some further analysis. In order to accomplish this, we emphasize in the present work a more direct effect on the shape and position of the spectra, namely, through the charging or decharging of the central atom where the core excitation takes place. A quantitative interpretation model for the shifts should account for both charging and polarization: charging in the initial ground state and polarization (relaxation) in the final state following the ionization. In fact, for inorganic and organometallic compounds, a ground-state charging model generally works well for predicting IP shifts, like the ESCA potential model[60] (the size of the final state polarization contribution, 1 eV, is very similar for every atom and is thus coped with by the general spectral alignment). The shift with respect to a reference level is in this model related to the charging of the central atom (multiplied by a so-called k parameter, given empirically or by the core valence Coulomb integral) and the charges of the surrounding atoms or atom groups divided by the interatomic distance to the central atom. Typically, the effect is dominated by the one-center contribution;[47] however, if coordination involves electronegative or electropositive groups at short distances, an essential contribution to the shift can be expected also from the coordinating atoms. The values of the IPEs for each Mn atom in the S_i clusters as a function of the charge on the same atom are shown in Figure 7. The general trend we have observed is that when an Mn atom is oxidized from (III) to (IV), its charge is enhanced by about +0.16 to +0.18 e$^-$. The effect of changes of the charges in the near surrounding of the metal is normally quite small, but this is not the case in the $S_2 \rightarrow S_3$ transition. The change of charge for
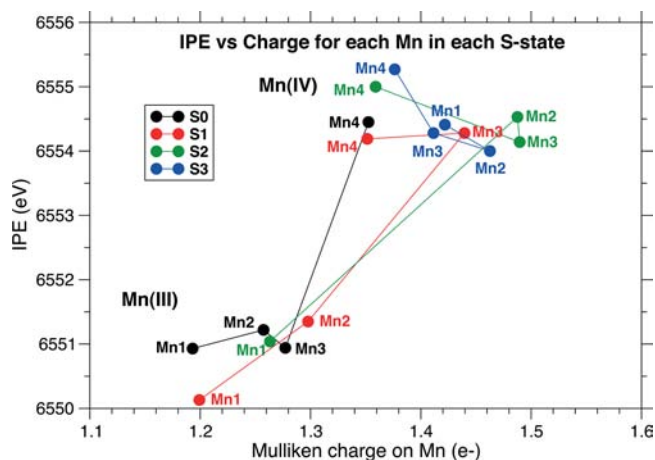
the oxidized atom (Mn1) is also in this case relatively large (+0.16 e$^-$). Following the empirical rules, this should lead to an IP shift of about +1.6 eV (assuming a k-factor of 10). However, in this transition an almost unbound neutral water ligand is deprotonated, forming a short Mn−OH bond to Mn1. The charge of this OH ligand is −0.30 and the Mn−OH distance is 1.78 Å. In its most simplified form this would lead to a contribution to the IP shift of −2.4 eV at Mn1, since the unbound water ligand in S_2 does not contribute at all, and this should be added to the +1.6 eV from the atom itself. From this simple analysis, the effect of the OH ligand could therefore in principle contribute significantly to both the position and shape of the curves. The reason the contribution from a ligand is so large in this case, which is unusual, is the loss of the Jahn−Teller axis in the transition, leading from 5- to 6-coordination. Admittedly, this is an oversimplified description but it still makes it understandable that the IPE shift might be observed as smaller in this transition than in the other ones. A more accurate charge distribution than just a single point charge on water would complicate the picture, as well as contributions from the other ligands on Mn1. Connecting to Dau's analysis,[58,59] we find that although a quantitative interpretation cannot be obtained in this simple way, this argument supports a notion that a different character of the NEXAFS curves for the $S_2 \rightarrow S_3$ transition can be understood even though a manganese oxidation occurs in this transition.

Direct time-dependent density functional theory (TDDFT) can also be used for core-level spectra.[25,61,62] A theoretical study of Mn K-edge NEXAFS based on TDDTF by Jaszewski et al.[25] proposes a "low" Mn oxidation state evolution, where the Mn$_4$ clusters follow a quite different oxidation pattern than obtained here, starting from S_0 (III, IV, II, II) to S_1 (III, IV, III, II) to S_2 (III, IV, III, III) and finally to S_3 (III, IV, IV, III). To analyze the present results in relation to the previous TDDFT results, it is important to address the different computer modeling techniques in some detail. A common view is that TD techniques have a clear advantage over static exchange (based on full hole or transition state optimized states) for valence electron excitations (where the word exchange cannot be interpreted literally in the case of most DFT functionals). The reason is that static exchange is a strict approximation (diagonal A Hessian matrix) with respect to TDHF (full A and B Hessian matrices) in the coupled perturbed (TD) equations. Although the availability of the B matrix in general makes only minor changes in excitation energies, it allows for a proper screening of the excitation (while static exchange energies are unscreened). It also allows for operator gauge invariance in a full basis set, which leads to "good quality" oscillator strengths also for limited basis sets, a major advantage for property calculations by TD methods. However, for core excitations the situation is completely different, something that follows from two neglected effects in TD methods: lack of orbital relaxation, which breaks the final state rule for NEXAFS,[63] and in the case of DFT, the electron self-interaction error, which is very large for core electrons. In fact these two effects are chemically dependent and have different sign, with the latter generally dominating. Thus TDDFT for manganese K excitations leads to some 70 eV offset error between the core orbital energy (or TDDFT excitation) and the IP, the exact value being subtly dependent on density functional, in particular the amount of exact exchange, and also chemical environment. Even a slight change in the core density, or change in the amount of exchange in the functional, has pronounced energetic

Figure 7. Computed IPEs of Mn atoms in the S states as a function of the charge in each Mn atom.

effects.[62,64] It was recently shown by one of the authors that chemical shifts in hydrogen-bonded systems could only be properly estimated by use of DFT core orbitals energies if these are self-energy-corrected.[65] Besley and Asmuruf[62] very recently presented an interesting analysis of the self-interaction error in TDDFT core excitation energies in terms of overlap character of the orbitals taking part in the excitations, much in the same manner as for the asymptotic behavior of DFT functionals for long-distance charge-transfer interactions. Problems arise in particular when the ground-state unoccupied orbital lacks an amplitude localized over the atom of the core hole. This makes the self-interaction-induced error large, when at the same time the relaxation-induced localization toward the opened core hole is neglected. Using the present static exchange technique, the core hole potential is preoptimized (or transition state is optimized, which is identical to ΔSCF energy up to the third order of perturbation theory). This technique includes orbital relaxation around the core hole (also in general increasing overlap), and avoids the self-energy problem that appears through core orbital energies. The result is an offset on the order of 1 eV (nonrelativistic) and thus well within the scale of general chemical shifts up to a few electronvolts, allowing for a fine assessment of spectral features in terms of small energy perturbations. The success of ΔSCF,[36] and somewhat more recently of ΔSCF Kohn−Sham[30,32] and of the transition-state approach, is a strong indicator of the preference for the use of orbital-optimized core potentials for calculating NEXAFS spectra.

CONCLUSIONS

The advent of modern synchrotron radiation sources and the concomitant development of computational methods for interpretation of X-ray spectra have made it possible to unravel important information on both structure and function of many biological systems. In the present work, near-edge X-ray absorption fine structure (NEXAFS) spectra have been analyzed for the active site of photosystem II (PSII), where water oxidation takes place. Particular focus has been placed on the method for assigning the oxidation states from the measured spectrum of the oxygen-evolving manganese complex. We have discussed our results both in view of earlier spectroscopic and theoretical work and in a general context of structure and functionality of the PSII system. Furthermore, in order to validate parametrizations—density functionals, basis set, and structural models—we carried out a set of calculations on a few manganese-containing complexes and compared them with available high-resolution spectra.

A major problem in the analysis of experimental NEXAFS spectra is the presence of overlapping atomic spectra for multinuclear clusters. Another problem is obviously that the manganese K-edge NEXAFS transitions occur at several thousands electronvolts while the separation of individual states requires a theoretical resolution of fractions of an electronvolt. At the same time the spectra are significantly broadened, homogeneously and in-homogeneously, by the underlying background that increases steeply above the IPE. In the present study a ΔSCF Kohn−Sham[30,32] method based on transition state has been used, in contrast to the previous study, which used the TDDFT method.[24,25] The present method was chosen on the bases of both its inherent superior properties and previous experience.[32,36] The static exchange spectrum is constructed from a fully optimized core hole or a transition potential, allowing inclusion of orbital relaxation around the

core hole and avoiding the electron self-energy problem, two factors that increase steeply as one moves down the main shells of an atom. This implies that one can maintain an offset on the order of an electronvolt (corrected for relativistic effects) well within the scale of chemical shifts that span a few electronvolts, allowing the addressing of spectral features in terms of chemical shifts and other small energy perturbations.

A major question in the analysis of the oxidation-state pattern of the OEC during water oxidation has been whether a manganese- or a ligand-centered oxidation occurs in the $S_2 \rightarrow S_3$ transition. Earlier studies have differed with respect to both the actual oxidation states and the assignment of where this oxidation is localized. The assignments have been made experimentally in terms of spectral analysis and theoretically in terms of optimization of geometries and electronic structure. In the present study, we have employed structural models for the S states obtained previously by energy minimization.[28] These structures were found to have a manganese-centered oxidation in each transition without any oxidation of ligands. We find that the NEXAFS-derived IPEs by the half-height method for S_0, S_1, S_2, and S_3 shift as 0.93, 1.43, and 0.63 eV, in reasonable agreement with experimental measurements by the same method of analysis. Any single Mn absorption spectrum is here characterized by a slightly different IPE and by a specific fine structure, determined by its local chemical environment. In the $S_2 \rightarrow S_3$ transition, a different character of the spectrum has been observed experimentally.[27,57] An analysis based on the charges and the potential model for core electron chemical shifts suggests that this is due to a change from 5- to 6-coordination following a loss of a Jahn−Teller axis, in line with a previous suggestion based on experiments,[58,59] and not due to a ligand oxidation.

One of the most important conclusions drawn from the present calculations is that the previously theoretically suggested structures and S-transitions[28] lead to NEXAFS (XANES) spectra in good agreement with experiments. Most interestingly, the IPE shift obtained for the $S_2 \rightarrow S_3$ transition is very small if the second-derivative method is used to identify the position of the IPE, in line with measurements,[57] but not if it is obtained by the half-height method, also in agreement with experiments.[27] The present analysis thus supports the assignments and structures suggested in the previous theoretical study based on energy minimization presented in ref 28. After the present study was initiated, a high-resolution structure of PSII has appeared[40] that also confirms the theoretical OEC structures with only small modifications.[66]

ASSOCIATED CONTENT

⑤ Supporting Information

Four tables listing atomic coordinates for S_0, S_1, S_2, and S_3 Mn complexes; complete ref 38. This material is available free of charge via the Internet at http://pubs.acs.org/.

AUTHOR INFORMATION

Corresponding Author

*E-mail barbara.brena@physics.uu.se.

Notes

The authors declare no competing financial interest.

ACKNOWLEDGMENTS

■ REFERENCES

(1) Stöhr, J. *NEXAFS Spectroscopy*; Springer−Verlag: Berlin, Heidelberg, New York, 1992.

(2) Hitchcock, A. P.; Tronc, M.; Modelli, A. *J. Phys. Chem.* **1989**, *93*, 3068−3077.

(3) Jordan-Sweet, J. L.; Kovac, C. A.; Goldberg, M. J.; Morar, J. F. *J. Chem. Phys.* **1988**, *89*, 2482−2489.

(4) Pettersson, L. G. M.; Ågren, H.; Schürmann, B. L.; Lippitz, A.; Unger, W. E. S. *Int. J. Quantum Chem.* **1997**, *63*, 749−765.

(5) Plashkevych, O.; Yang, L.; Vahtras, O.; Ågren, H.; Petterson, L. G. M. *Chem. Phys.* **1997**, *222*, 125−137.

(6) Carravetta, V.; Plashkevych, O.; Ågren, H. *J. Chem. Phys.* **1998**, *109*, 1456−1464.

(7) Plashkevych, O.; Carravetta, V.; Vahtras, O.; Ågren, H. *Chem. Phys.* **1998**, *232*, 49−62.

(8) Yang, L.; Plashkevytch, O.; Vahtras, O.; Carravetta, V.; Ågren, H. *J. Synchrotron Radiat.* **1999**, *6*, 708−710.

(9) Kaznacheyev, K.; Osanna, A.; Jacobsen, C.; Plashkevych, O.; Vahtras, O.; Ågren, H.; Carravetta, V.; Hitchcock, A. P. *J. Phys. Chem. A* **2002**, *106*, 3153−3168.

(10) Kirtley, S. M.; Mullins, O. C.; Chen, J.; van Elp, J.; George, S. J.; Chen, C. T.; O'Halloran, T.; Cramer, S. P. *Biochim. Biophys. Acta* **1992**, *1132*, 249−254.

(11) MacNaughton, J. B.; Moewes, A.; Lee, J. S.; Wettig, S. D.; Kraatz, H. B.; Ouyang, L. Z.; Ching, W. Y.; Kurmaev, E. Z. *J. Chem. Phys.* **2006**, *110*, 15742−15748.

(12) MacNaughton, J. B.; Kurmaev, E. Z.; Finkelstein, L. D.; Lee, J. S.; Wettig, S. D.; Moewes, A. *Phys. Rev. B* **2006**, *73*, 205114.

(13) Kato, H. S.; Furukawa, M.; Kawai, M.; Taniguchi, M.; Kawai, T.; Hatsui, T.; Kosugi, N. *Phys. Rev. Lett.* **2004**, *93*, 086403.

(14) Harada, Y.; Takeuchi, T.; Kino, H.; Fukushima, A.; Takakura, K.; Hieda, K.; Nakao, A.; Shin, S.; Fukuyama, H. *J. Phys. Chem. A* **2006**, *110*, 13227−13231.

(15) Furukawa, M.; Kato, H. S.; Taniguchi, M.; Kawai, T.; Hatsui, T.; Kosugi, N.; Yoshida, T.; Aida, M.; Kawai, M. *Phys. Rev. B* **2007**, *75*, 045119.

(16) Hua, W.; Gao, B.; Li, S.; Ågren, H.; Luo, Y. *J. Phys. Chem. B* **2010**, *114*, 13214−13222.

(17) Ferreira, K. N.; Iverson, T. M.; Maghlaoui, K.; Barber, J.; Iwata, S. *Science* **2004**, *303*, 1831−1838.

(18) Loll, B.; Kern, J.; Saenger, W.; Zouni, A.; Biesiadka, J. *Nature* **2005**, *438*, 1040−1044.

(19) Guskov, A.; Kern, J.; Gabdulkhakov, A.; Broser, M.; Zouni, A.; Saenger, W. *J. Nat. Struct. Biol.* **2009**, *16*, 334−341.

(20) Siegbahn, P. E. M. *Chem.—Eur. J.* **2008**, *27*, 8290−8302.

(21) Kok, B.; Forbush, B.; McGloin, M. *Photochem. Photobiol.* **1970**, *11*, 457−475.

(22) Yano, J.; Yachandra, V. K. *Photosynth Res.* **2007**, *92*, 298−303.

(23) Yachandra, V. K.; Sauer, K.; Klein, M. P. *Chem. Rev.* **1996**, *96*, 2927−2950.

(24) Jaszewski, A. R.; Stranger, R.; Pace, R. J. *J. Phys. Chem. A* **2008**, *112*, 11223−11234.

(25) Jaszewski, A. R.; Petrie, S.; Stranger, R.; Pace, R. J. *Chem.—Eur. J.* **2011**, *17*, 5699−5713.

(26) Messinger, J.; Robblee, J. H.; Bergmann, U.; Fernandez, C.; Glatzel, P.; Visser, H.; Cinco, R. M.; McFarlane, K. L.; Bellacchio, E.; Pizarro, S. A.; Cramer, S. P.; Sauer, K.; Klein, M. P.; Yachandra, V. K. *J. Am. Chem. Soc.* **2001**, *123*, 7804−7820.

(27) Iuzzolino, L.; Dittmer, J.; Dörner, W.; Meyer-Klaucke, W.; Dau, H. *Biochemistry* **1998**, *37*, 17112−17119.

(28) Siegbahn, P. E. M. *Acc. Chem. Res.* **2009**, *42*, 1871−1880.

(29) Slater, J. C. *Quantum Theory of Molecules and Solids*, Vol. *IV*; McGraw-Hill: New York, 1974.

(30) Chong, D. P. *Chem. Phys. Lett.* **1995**, *232*, 486−490.

(31) Stener, M.; Lisini, A.; Decleva, P. *Chem. Phys.* **1995**, *191*, 141−154.

(32) Triguero, L.; Plashkevych, O.; Pettersson, L. G. M.; Ågren, H. *J. Electron. Spectrosc. Relat. Phenom.* **1999**, *104*, 195−207.

(33) Nyberg, M.; Luo, Y.; Triguero, L.; Pettersson, L. G. M.; Ågren, H. *Phys. Rev. B* **1999**, *60*, 7956−7960.

(34) Guo, J.-H.; Luo, Y.; Augustsson, A.; Kashtanov, S.; Rubensson, J.-E.; Shuh, D. K.; Ågren, H.; Nordgren, J. *Phys. Rev. Lett.* **2003**, *91*, No. 157401.

(35) Cavalleri, M.; Nåslund, L.-Å.; Edwards, D. C.; Wernet, P.; Ogasawara, H.; Myneni, S.; Ojamåe, L.; Odelius, M.; Nilsson, A.; Pettersson, L. G. M. *J. Chem. Phys.* **2006**, *124*, No. 194508.

(36) Ågren, H.; Carravetta, V.; Vahtras, O.; Pettersson, L. G. M. *Theor. Chem. Acc.* **1997**, *97*, 14−40.

(37) Yachandra, V. K.; DeRose, V. J.; Latimer, M. J.; Mukerji, I.; Sauer, K.; Klein, M. P. *Science* **1993**, *260*, 675−679.

(38) Frisch, M. J., et al. Gaussian 09, Revision A.1; Gaussian, Inc., Wallingford, CT, 2009.

(39) Becke, A. D. *J. Chem. Phys.* **1993**, *98*, 5648−52.

(40) Umena, Y.; Kawakami, K.; Shen, J.-R.; Kamiya, N. *Nature* **2011**, *473*, 55−60.

(41) Schrödinger, LLC. Jaguar 5.5, Portland, OR 1991−2003.

(42) Hermann, K. et al. StoBe-deMon version 3.0, 2007.

(43) Becke, A. D. *Phys. Rev. A* **1988**, *38*, 3098−3100.

(44) Perdew, J. P. *Phys. Rev. B* **1986**, *33*, 8822−8824.

(45) Triguero, L.; Pettersson, L. G. M.; Ågren, H. *Phys. Rev. B* **1998**, *58*, 8097−8110.

(46) Kutzelnigg, W.; Fleischer, U.; Schindler, M. *NMR Basic Principles and Progress*; Springer−Verlag, Heidelberg, Germany, 1990; Vol. 23, p 16.

(47) Gelius, U. *Phys. Scr.* **1974**, *9*, 133−147.

(48) Ågren, H. *Int. J. Quantum Chem.* **1991**, *39*, 455−486.

(49) Medinallanos, C.; Ågren, H.; Mikkelsen, K. V.; Jensen, H. *J. Chem. Phys.* **1989**, *90*, 6422−6435.

(50) Blomberg, M. R. A.; Siegbahn, P. E. M. *Theor. Chem. Acc.* **1997**, *97*, 72−80.

(51) Siegbahn, P. E. M. *Curr. Opin. Chem. Biol.* **2002**, *6*, 227−235.

(52) Visser, H.; Anxolabehere-Mallart, E.; Bergmann, U.; Glatzel, P.; Robblee, J. H.; Cramer, S. P.; Girerd, J. J.; Sauer, K.; Klein, M. P.; Yachandra, V. K. *J. Am. Chem. Soc.* **2001**, *123*, 7031−7039.

(53) Yachandra, V. K.; DeRose, V. J.; Latimer, M. J.; Sauer, K.; Klein, M. P. *Jpn. J. Appl. Phys.* **1993**, *32*, 523−526.

(54) de Groot, F.; Vankó, G.; Glatzel, P. *J. Phys.: Condens. Matter* **2009**, *21*, No. 104207.

(55) Penner-Hahn, J. E.; Fronko, R. M.; Pecoraro, V. L.; Yochum, C. F.; Betts, S. D.; Bowlby, N. R. *J. Am. Chem. Soc.* **1990**, *112*, 2549−2557.

(56) Ono, T.; Noguchi, T.; Inoue, Y.; Kusunoki, M.; Matsushita, T.; Oyanagi, H. *Science* **1992**, *258*, 1335−1337.

(57) Roelofs, T. A.; Liang, W.; Latimer, M. J.; Cinco, R. M.; Rompel, A.; andrews, J. C.; Sauer, K.; Yachandra, V. K.; Klein, M. P. *Proc. Natl. Acad. Sci. U.S.A.* **1996**, *93*, 3335−3340.

(58) Dau, H.; Liebisch, P.; Haumann, M. *Anal. Bioanal. Chem.* **2003**, *376*, 562−583.

(59) Dau, H.; Liebisch, P.; Haumann, M. *Phys. Scr.* **2005**, *T115*, 844−846.

(60) Siegbahn, K.; Nordling, C.; Johansson, G.; Hedman, J.; Hedén, P. F.; Hamrin, K.; Gelius, U.; Bergmark, T.; Werme, L. O.; Manne, R.; Baer, Y. *ESCA applied to free molecules*; North-Holland Publishing Co.: Amsterdam, 1969.

(61) Guangde, T.; Rinkevicius, Z.; Vahtras, O.; Ågren, H.; Ekström, U.; Norman, P. *Phys. Rev. A* **2007**, *76*, No. 022506.

(62) Besley, N. A.; Asmuruf, F. A. *Phys. Chem. Chem. Phys.* **2010**, *12*, 12024−12039.

(63) Privalov, T.; Gel'mukhanov, F.; Ågren, H. *Phys. Rev. B* **2001**, *64*, No. 165116.

(64) Guangde, T.; Carravetta, V.; Vahtras, O.; Ågren, H. *J. Chem. Phys.* **2007**, *127*, No. 174110.

(65) Tu, G.; Tu, Y.; Vahtras, O.; Ågren, H. *Chem. Phys. Lett.* **2008**, *468*, 294−298.

(66) Siegbahn, P. E. M. *ChemPhysChem* **2011**, *12*, 3274−3280.